REVIEW OF BALLISTIC LIMIT EQUATIONS FOR CFRP STRUCTURE WALLS OF SATELLITES

Frank Schäfer[(1)], Eberhard Schneider[(1)], Michel Lambert [(2)]

[(1)]Fraunhofer-Institut für Kurzzeitdynamik, Ernst-Mach-Institute (EMI),Eckerstr. 4, D- 79104 Freiburg, Germany, Email: schaefer@emi.fhg.de, schneider@emi.fhg.de
[(2)]ESA-ESTEC, Postbus 299, NL-2200 AG Noordwijk, The Netherlands, Email: michel.lambert@esa.int

ABSTRACT

In this paper a review of existing ballistic limit equations for CFRP (Carbon Fibre Reinforced Plastics) structure walls of satellites is given, and two new ballistic limit equations are presented. The predictive capabilities of the equations are compared to a set of experimental hypervelocity impact test data of CFRP plates and CFRP honeycomb sandwich panels (satellite structure wall) from ENVISAT, AXAF, and a generic technology program.

In the literature, three ballistic limit equations for sandwich panels (SP) made from CFRP face-sheets and Al- honeycomb (H/C) core were found and analyzed (Frost's approach, Approach using Christiansen's Whipple shield Ballistic Limit Equation (BLE), and Taylor's approach). Furthermore, in this paper, a new ballistic limit equation was proposed for CFRP H/C SP (Modified ESA Triple Wall Equation) and for composite panels (plates) with and without MLI attached to the surface.

The amount of impact data on CFRP structure walls of satellites found in the literature was rather scarce. The new BLE for CFRP plates makes good predictions to the available set of test data. For the BLE for CFRP H/C SP, it was found that Frost's approach and application of Christiansen's BLE to CFRP H/C SP lead to an overprediction of the ballistic limit diameters for ENVISAT structure walls and the samples of the generic technology program. Taylor's approach and the newly designed MET ballistic limit equation have both yielded good predictions for all samples except for the AXAF samples that had rather thin-walled face-sheets and a thin Al H/C core: for these samples the predictions were conservative. Thus, for use in risk analysis tools for satellites (e. g. ESA's ESABASE/DEBRIS tool or NASA's BUMPER code), it is recommended to use either the MET or Taylor equation.

1. NOTATION & ACRONYMS

d_c	critical particle diameter causing failure of the sample [cm]
D_{eq}	equivalent circular hole dia. in the rear face-sheet calculated from the projected area of the clear hole in the sample [mm]
k	constant describing type of failure (k = 1.8 for "no hole" failure criterion in CFRP plates; k = 3.0 for "no detached spall" failure criterion)
K2	Fit factor describing protection enhancement introduced by MLI [-]
K_{CFRP}	fit constant for CFRP in single wall penetration equation [-]
S	inner spacing between bumper and back wall of a Whipple Shield [cm]
t_{CFRP}	thickness of the CFRP plate [cm]
$t_{F/S}$	thickness of the face-sheets of a H/C SP [cm]
$t_{F/S,CFRP}$	thickness of CFRP face-sheet of CFRP H/C SP [cm]
$t_{H/C}$	thickness of honeycomb core [cm]
t_w	rear wall thickness [cm]
v	projectile velocity [km/s]
v_n	component of the impact velocity normal to the target surface ($v_n = v \cdot \cos\theta$) [km/s]
$\rho_{AD,MLI}$	surface density of the MLI [g/cm^2]
ρ_b	bumper density [g/cm^3]
ρ_{CFRP}	volumetric density of CFRP [g/cm^3]
ρ_p	projectile density [g/cm^3]
θ	impact angle, measured from the surface normal of the target plate [°]
σ, σ_y	yield strength of the rear wall of a Whipple Shield [ksi]
$\sigma_{y,CFRP}$	yield strength of CFRP [ksi]
σ_U	ultimate tensile strength [ksi] or [MPa]

Al	Aluminium
BLC	Ballistic Limit Curve
BLE	Ballistic Limit Equation
CFRP	Carbon-Fibre Reinforced Plastics
CFRP H/C SP	Honeycomb Sandwich panel with CFRP face-sheets and Al-H/C core
ETW	ESA Triple Wall Equation
H/C	honeycomb
HVI	Hypervelocity Impact
MET	Modified ESA Triple Wall Equation
SP	sandwich panel
w/o	without

To be published in: PROCEEDINGS OF THE 5th INTERNATIONAL SYMPOSIUM ON ENVIRONMENTAL TESTING FOR SPACE PROGRAMMES, 15.-17. June 2004, ESA-ESTEC, Noordwijk, The Netherlands, ESA SP-558

2. INTRODUCTION

Carbon Fiber Reinforced Plastic (CFRP) materials are increasingly used in satellite applications, for example as satellite structural elements (sandwich panels with thin face-sheets from CFRP and Al-honeycomb core), or for baffles or platforms (CFRP sheet material). The benefit of using CFRP for structural applications is firstly due to their low coefficient of thermal expansion and secondly due to the high stiffness that can be reached at low surface weight.

However, there is a drawback to the use of CFRP on satellites: this class of materials has a low protection performance with regards to hypervelocity impacts from space debris and meteoroids. Furthermore, in case of a penetration, besides the mechanical impact damages that may lead to destruction of critical spacecraft components (harness, E-boxes etc.), large amounts of fibres are also ejected into the interior of the satellite. These electrically conducting fibres may trigger electrical perturbations such as discharges.

In order to assess the risk associated with meteoroid and space debris impacts on satellite components, the ballistic limit curve of the respective structure wall has to be known. The ballistic limit curve gives the "critical projectile diameter" d_c as a function of impact velocity and impact angle for a certain spacecraft structure. The "critical projectile diameter" d_c is defined as the projectile diameter that penetrates a given structure wall as a function of impact velocity and thus can cause damage to satellite subsystems.

It is mandatory to understand the effects that occur under hypervelocity impacts to allow for appropriate design countermeasures. This article begins by explaining the effects of hypervelocity impact on relevant structures, then an analysis on existing ballistic limit equations is performed and new ballistic limit equations are presented. Finally the predictive capabilities of the equations are investigated.

3. HYPERVELOCITY IMPACT TESTING OF CFRP STRUCTURES

3.1 Phenomenological description of hypervelocity impact damages in CFRP structures

CFRP plates

The main damages in CFRP plates caused by impact of projectiles at velocities of several kilometres per second are: fibre breaking, matrix breakage, and layer delaminations (for example see Fig. 1 and Fig. 2). Commonly, as shown in Fig. 1, the crater or the perforation hole in the plate is of irregular, roughly circular shape. The edges of the crater or perforation holes are composed of fractured fibre strands. Typically, in the vicinity of the impact location, severe de-bonding of the laminated layers occurs. In a localized zone around the impact hole, part of the surface layer is spalled off, delaminated or cracked. Fibre protrusion can also be observed. Delaminations of the composite layers typically extend beyond the measurable damage extension: they have to be determined through ultrasonic scanning and are not visible in Fig. 1 and Fig. 2. Cracks typically occur in the surface layers. The crack propagation direction is consistent with the weaving pattern of the fabric.

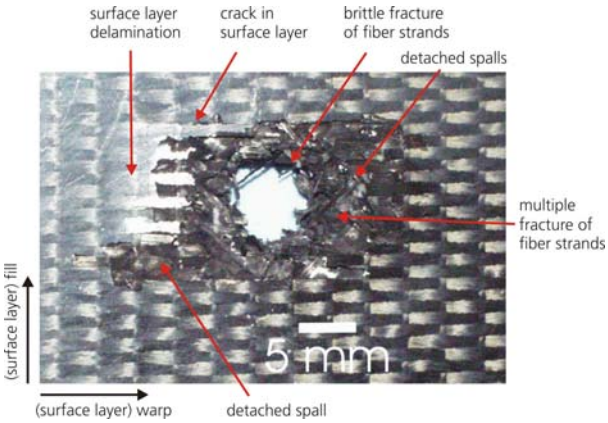

Fig. 1. EMI Exp. No. 4277 (front side); target: 3.8 mm thick CFRP plate (description see Chapter 3.2); projectile: 3 mm Al-sphere at 4550 m/s normal impact

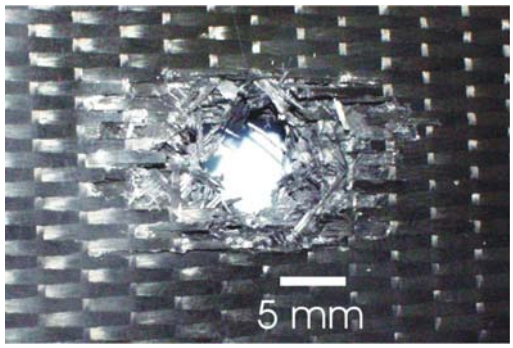

Fig. 2. EMI Exp. No. 4277 (rear side)

Honeycomb Sandwich panels with CFRP face-sheets

The principal damages observed in the front face-sheet of an Al-honeycomb sandwich panel with CFRP face-sheets are similar to the damages observed in CFRP plates as described above (Fig. 4, top). In the Al-honeycomb core, basically three different honeycomb cell damages can be distinguished: deformation and crushing of the honeycomb cells, perforation of the honeycomb cells, and complete disintegration of the honeycomb cells (Fig. 3). The damaged honeycomb volume is typically tube-like or conical in shape. In the vicinity of the shot axis, the

honeycomb cells are severely fragmented, sometimes described as "disintegrated". Further away from the shot axis the cells are perforated by off-axis projectile fragments and are deformed or crushed. At lower velocity impact ("low velocity" being defined as an impact velocity not resulting in severe projectile fragmentation on the front face-sheet, here: about 3 km/s), at oblique impacts, and at impacts of projectiles having dimensions similar to the honeycomb cell size, the discreteness of the honeycomb core influences drastically the type and extent of the honeycomb damage. The discreteness of the honeycomb structure is of decreasing influence when the diameter of the impacting projectile increases, because the larger the projectile diameter and the higher the impact velocity, the larger the damage area in the honeycomb core. Thus, the core behaves like a continuum.

The principal damages observed in the rear face-sheet of a honeycomb sandwich panel with CFRP face-sheets may differ from the damages observed in the front face-sheets. In case of complete perforation of the rear face-sheet (Fig. 4, bottom), typically the extension of spalled areas and delaminations is larger than those observed in the front face-sheets. Also, through-going cracks are observed. In the case when impact conditions are close to the ballistic limit of the CFRP honeycomb sandwich panel, detached spallations and pinholes are observed.

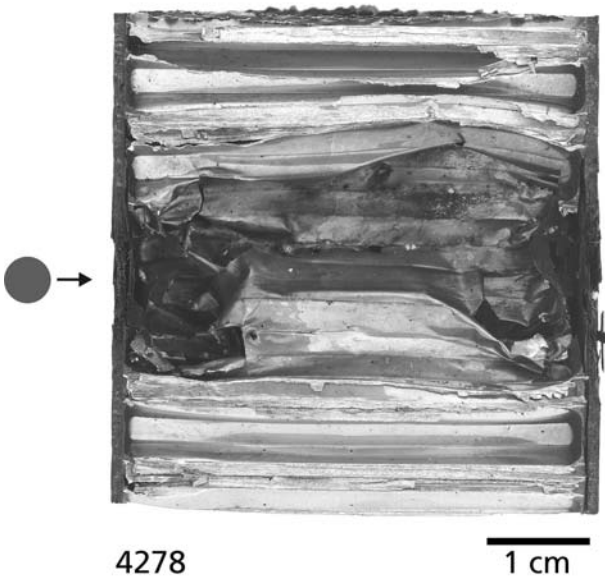

Fig. 3. EMI Exp. No. 4278; target: CFRP H/C SP, section (face-sheets: 1.1 mm CFRP, Al-H/C core: 45 mm thick, target description see Chapter 3.2); projectile: 3 mm Al-sphere at 4490 m/s normal impact

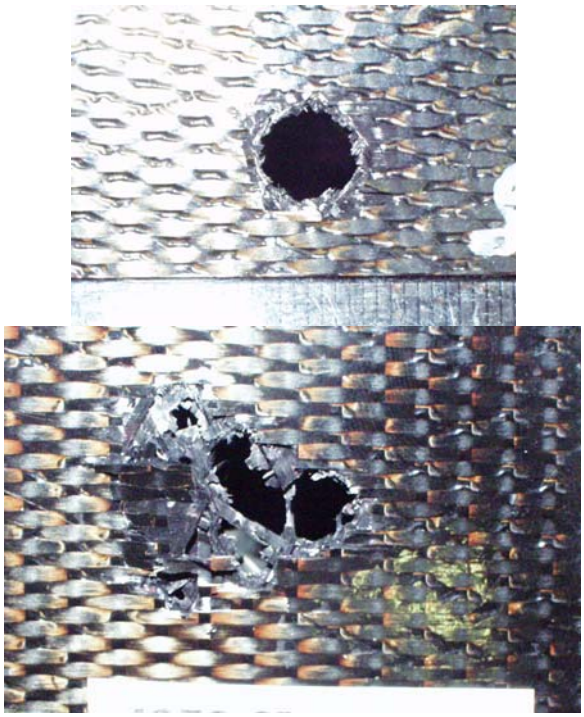

Fig. 4. EMI Exp. No. 4278, front (top) and rear (bottom) face-sheet of CFRP honeycomb sandwich panel from Fig. 3

3.2 Impact Test Data used in this paper

Data from hypervelocity impact tests on CFRP plates

In [1], hypervelocity impact tests, performed on CFRP plates at Ernst-Mach-Institute [2] are summarized. Two configurations have been tested: CFRP plates without MLI and CFRP plates with MLI. The CFRP plates were 3.8 mm thick, made of carbon fibre fabric (Brochier GB305 and GB230) with epoxy resin (Brochier LY564, RTM 120°C). The CFRP plate consisted of 12 plies, with a lay-up as follows ($^{(1)}$ and $^{(2)}$: see Fig. 5): $(0^{(1)}/45^{(2)}/0^{(1)}/0^{(1)}/45^{(2)}/0^{(1)}/0^{(2)}/45^{(2)}/0^{(1)}/0^{(1)}/45^{(2)}/0^{(1)})$. The fiber volume was 60 %.

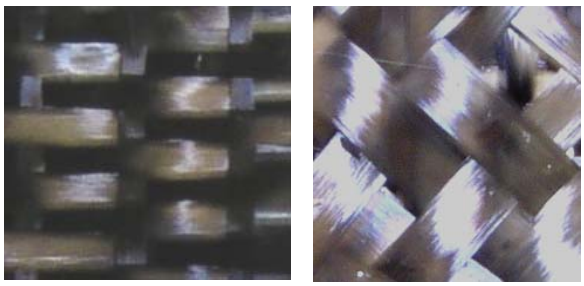

Fig. 5. Weaving pattern of the $^{(1)}$ and $^{(2)}$ numbered layers of the above 3.8 mm CFRP plate (pictures approx. same scale)

The material surface density was 0.54 g/cm^2, the volumetric density of the composite was 1.42 g/cm^3. The MLI was composed of one 75 µm layer of aluminized Kapton, 20 layers of aluminized Kapton (7.5 µm thick) separated by thin Dacron nets (170 µm) and a rear layer of Kapton reinforced Nomex (125 µm thick). The surface density of the complete MLI was 0.058 g/cm^2.

Three impact tests have been performed on the samples without MLI, four impact tests on the samples with MLI (Table 1). All impact tests have been performed with aluminium spherical projectiles at velocities around 6 km/s, impacting normal to the target surface.

Table 1. Test matrix for impact tests on 3.8 mm thick CFRP plates without and with MLI (from [1] and [2]).

EMI No.	Tar-get	ρ_p	d_p	v	damage description
		[g/cm^3]	[mm]	[km/s]	
2237	(1)	2.7	0.71	6.2	small detached spall zone on rear side
2249	(1)	2.7	1.22	6.0	clear perforation hole
2262	(1)	2.7	0.90	6.0	tiny perforation hole
2264	(2)	2.7	0.92	6.3	detached spallation
2271	(2)	2.7	1.20	5.8	small perforation hole
2276	(2)	2.7	1.02	6.1	detached spallation
2278	(2)	2.7	1.10	6.6	small hole

Note: (1) 3.8 mm CFRP; (2) 3.8 mm CFRP + MLI

Other impact data that were analyzed in this paper stem from impact tests on CFRP tubes [3]. The target description according to [3] is: Tube length 500 ± 1 mm, Outer dia.: 35.5 ± 0.3 mm, Inner dia. 33 ± 0.1 mm, Fibre T300 for 90°, M40 for 0°, Fiber Content 66% in volume, Layup 90°/0°/90°, Space Approved Epoxy. The manufacture was filament winding, vacuum impregnation, surface ground.

Table 2. Test matrix for impact tests on CFRP struts/tubes (from [3], tests were performed at EMI)

Test No.	Tar-get	ρ_p	d_p	v	damage description
		[g/cm^3]	[mm]	[km/s]	
2559	(1)	2.7	0.90	7.5	front wall of strut perforated (3.7 mm avg. hole dia.)
1422	(2)	2.7	0.90	2.6	front wall of strut perforated (2.0 mm square hole dia.)

Note: (1) 2.62 mm thick CFRP strut, inner dia. 32.98 mm; (2) 2.73 mm thick CFRP strut, inner dia. 32.98 mm

Data from hypervelocity impact tests on sandwich panels with CFRP face-sheets and Al-honeycomb core

In [4], hypervelocity impact tests on ENVISAT H/C SP with CFRP face-sheets at normal incidence are reported. According to this reference, the face-sheets are 1.10 mm thick and are made of CFRP fibres M40 and NCHM914 epoxy resin with a quasi-orthotropic lay-up (3x(0,+/- 60)). The Al-honeycomb core (type 3/16-.0015-5056 P) is 45 mm thick. Surface density of the SP is 7.4 kg/m^2. MLI consisted of 21 layers of Mylar with 20 intermediate Dacron spacers. The areal density of this MLI was 0.0560 g/cm^2. The experiments are listed in Table 3.

Table 3. Test matrix and results of impact tests on ENVISAT H/C SP with CFRP face-sheets and Al-H/C core without and with MLI (from [4]).

EMI No.	Tar-get	ρ_p	d_p	v	damage
		[g/cm^3]	[mm]	[km/s]	(in rear CFRP face-sheet)
2295	(1)	2.7	0.90	6.60	no spall
2287	(1)	2.7	1.10	5.30	hole + spall
2285	(1)	2.7	1.10	6.30	spall
2306	(2)	2.7	1.10	6.50	no spall
2312	(2)	2.7	1.50	6.40	cracks+spall

Note: (1) CFRP face-sheets 1.10 mm thick, Sandwich-Panel with Al-Honeycomb-Core, 45 mm thick; (2) same as (1) + MLI

In [5], hypervelocity impact tests on sandwich structures consisting of CFRP face-sheets with Al-honeycomb core are reported. A few results from impact tests at normal projectile incidence were used in this paper (Table 4). The equivalent diameter D_{eq} represents a clear hole in the rear face-sheet which has the same projected area as the actual hole measured in the sample. The sandwich structure was described in [5] as follows: Prepreg matrix was 4-ply satin woven carbon fibre epoxy HMF371-7714B, lay-up was (0°/90°/90°/0°), with a thickness of 1.62 mm. The density of the composite face-sheets was 1.80-1.85 g/cm³. The H/C core was from Aeroweb, Al alloy 3003, having a core density of 83 kg/m³, and a cell size of 6.4 mm (0.25 in.). The cell foil thickness was 0.06 mm (25*10^{-4} in). Thickness of the core was 45 mm.

Table 4. Test matrix and results of impact tests on H/C SP with CFRP face-sheets and Al-H/C core (from [5]).

EMI No.	Tar-get	ρ_p	d_p	v	damage description
		[g/cm^3]	[mm]	[km/s]	(in rear CFRP face-sheet)
HC15	(1)	2.78	1.00	5.42	no rear perforation
HC16	(1)	2.78	1.20	4.86	perforation, D_{eq} = 1.80 mm
HC17	(1)	2.78	1.50	5.93	perforation, D_{eq} = 4.77 mm
HC18	(1)	2.78	2.00	5.08	perforation, D_{eq} = 6.45 mm

Note: (1) Sandwich-Panel with Al-Honeycomb-Core, 45 mm thick, CFRP face-sheets 1.62 mm thick

Data from impact tests performed on AXAF structure wall samples could be identified in the literature [6]. All impacts were normal to the structure wall. The samples were described as follows: Sandwich panel with CFRP face-sheets P100 (0.762 mm thick) and Al-honeycomb core (15.875 mm thick with cell diameter of 3.175 mm). The sample design differs considerably from the design of the two other CFRP H/C SP presented previously. MLI consists of a silver/teflon/inconel laminate cover layer bonded to an outer layer of aluminized Kapton, 22 filler layers of aluminized Kapton, 23 separator layers of Dacron, and an inner layer of aluminized Kapton.

Table 5. Test matrix and results of impact tests on H/C SP with CFRP face-sheets and Al-H/C core + MLI (from [6]).

Test No.	Target	ρ_p	d_p	v	damage description
		[g/cm^3]	[mm]	[km/s]	
A-2636	(1)	2.79	1.59	6.65	"failed" = rear face-sheet penetration
A-2637	(1)	2.79	1.19	6.80	"passed" = no rear face-sheet penetration

Note: (1) CFRP face-sheets 0.762 mm thick, Sandwich-Panel with Al-Honeycomb-Core, 15.875 mm thick

4. BALLISTIC LIMIT EQUATION FOR CFRP STRUCTURE WALLS OF SATELLITES

4.1 Ballistic Limit Equation for CFRP Panels with and without MLI

For CFRP panels no ballistic limit equation was found in the literature. This is attributed to the fact that composite panels are rarely space-facing and thus are seldom impacted by hypervelocity particles.

For CFRP panels, a new ballistic limit equation is proposed here (Eq. (1)):

$$d_c = \frac{t_{CFRP} + K2 \cdot \frac{\rho_{AD,MLI}}{\rho_{CFRP}}}{k \cdot K_{CFRP} \cdot \rho^{\alpha} \cdot v_n^{\beta}} \qquad (1)$$

The ballistic limit equation yields the critical projectile diameter d_c leading to failure of an impacted CFRP plate as a function of the normal component of impact velocity v_n. The projectile is a sphere having density ρ. The plate has a thickness t_{CFRP}. The factor K_{CFRP} is a constant of the material (CFRP). It is fit once to impact test data for one type of CFRP and then kept constant. The type of failure (described by dimensionless factor k) is: (a) detached spall/no clear hole, and (b) clear hole. The ballistic limit equation is similar to a ballistic limit equation originally proposed by Cour-Palais for thin metallic plates (so-called "Cour-Palais Thin Plate equation" [7]). It contains a few generic coefficients which can be fit to experimental results. For the coefficients α and β the values of the Cour-Palais thin plate equation (0.5 for α, 2/3 for β) were selected. It is reasonable to assume that the principal dependence of the critical diameter on the parameters of the equation for CFRP plates should be somewhat similar to the coefficients used for the ballistic limit equation of metallic plates. The factor K2 describes the protection enhancement gained from using MLI on top of the CFRP plate. MLI effectively increases the ballistic limit diameter. For K2, a factor of 4.5 was fit to impact tests on Al-plates with MLI placed on top. This factor was adopted for MLI used on CFRP plates. The K2 factor has to be interpreted such that addition of MLI effectively increases the thickness of the CFRP plate by a factor of 4.5 compared to the equivalent CFRP thickness which corresponds to the surface weight of MLI.

As the number of hypervelocity impact test data available for analysis is rather limited, it is not yet possible to include in the equation the dependence of the ballistic limit diameter on fibre type, fibre/matrix volume content, weave type, lay-up etc. These factors are included at the moment in the parameter K_{CFRP}.

For the “no hole” failure criterion the same factor k as used for metals was selected (k = 1.8, see also [7]). For the failure criterion “no detached spall” the factor k was selected larger than the value used in [7] due to the increased brittleness of CFRP compared to metals. In order to describe this type of failure, a factor of k = 3.0 was assumed, because no corresponding experimental data for fitting this case was available (all available test results were perforations resulting in clear hole damages in the CFRP plates, see Table 1 and Table 2). Thus, verification of the k-factor remains to be done in future impact tests.

Using the experimental hypervelocity impact test data listed in Table 1 and Table 2, K_{CFRP} was fit to 0.52. In Table 6, the whole set of data to be used with Eq. (1) is listed.

Table 6. Values to be used with Eq. (1) when applied to CFRP plates with and without MLI

para-meter	description	Value to be used with Eq. (1)
K2	Fit factor descr. the protection enhance-ment of MLI [-]	4.5
α	Density coefficient [-]	0.5
β	Velocity coefficient [-]	2/3
K_{CFRP}	constant describing the target material	0.52
k	constant describing type of failure	for CFRP "no hole" criterion k = 1.8 for CFRP "no detached spall" criterion k =3.0

4.2 Comparison of the predictions made by the BLE for CFRP Panels with experimental data

The ballistic limit curves are plotted versus the impact test data given in Fig. 6 and Fig. 7. The values used to generate the ballistic limit curve plots are listed in Table 7.

Table 7. Parameters used for BLC calculations for CFRP plates with and without MLI using Eq. (1), x = applies (see Fig. 6 - Fig. 7)

MLI	→	no	no	yes	yes
failure criterion	→	no hole	no spall	no hole	no spall
variable	**value**				
θ	0	x	x	x	x
t_{CFRP}	0.380 cm	x	x	x	x
ρ	2.70 g/cm³	x	x	x	x
k	1.80	x		x	
k	3.0		x		x
ρ_{CFRP}	1.8 g/cm³			x	x
$\rho_{AD,MLI}$	0.058 g/cm²			x	x

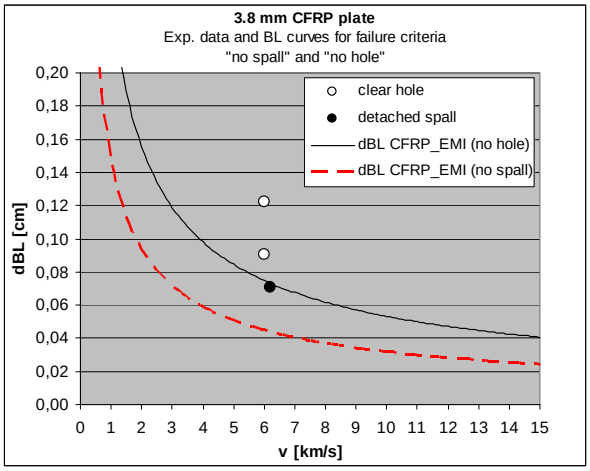

Fig. 6. Impact test data of CFRP plates (Table 1) and BLC for failure criteria “no hole” and “no spall”

The interpretation of the curves is as follows (example, Fig. 6): When a 3.8 mm thick CFRP plate is impacted at a velocity of 7 km/s at normal incidence with an Al-sphere, up to a projectile diameter of up to 0.4 mm no spall damage in the rear side of the plate would be expected. Impact of projectiles having diameters between 0.4 mm and ca. 0.7 mm would result in detached spall from the rear side of the CFRP plate. The spalled material is ejected into the half-space behind the plate, resulting in contamination of the spacecraft’s interior through conductive CFRP fibres. When impacted with projectiles having diameters larger than 0.7 mm, complete perforation resulting in a clear hole would be expected. In this case, projectile fragments and carbon fibres would be ejected into the half-space behind the CFRP plate. Thus, besides contamination with finely fragmented fibers, impact damages from the Al-projectile fragments could be expected.

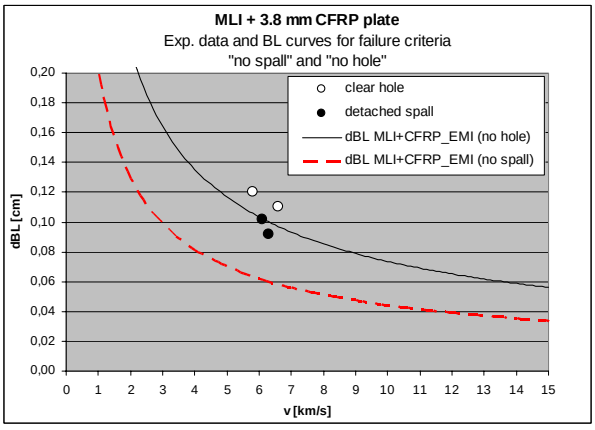

Fig. 7. Impact test data of CFRP plates covered with MLI (Table 1) and BLC for failure criteria “no hole” and “no spall”

In Fig. 8, the impact data from the hypervelocity impact tests on the CFRP strut (Table 2, [3]) are displayed

using Eq. (1). The predictions from Eq. (1) are good, although, the test result at lower velocity is slightly overpredicted.

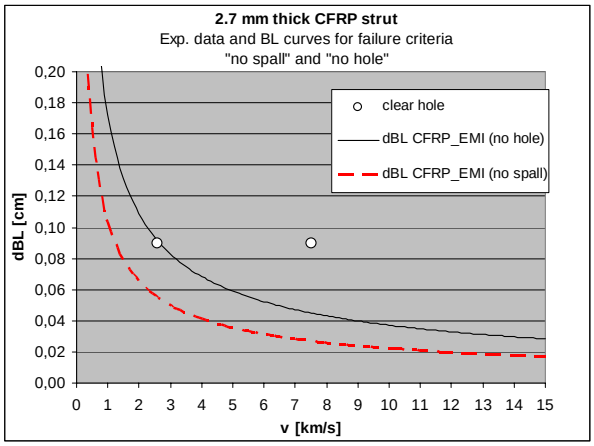

Fig. 8. Impact test data of CFRP plates (Table 2) and BLC for failure criteria “no hole” and “no spall”

Of course Eq. (1) needs further experimental validation. Especially, no experimental verification of the impact angle dependence has yet been made.

Summarizing, the equation is presently verified for CFRP having thicknesses in the range of 2.7 to 3.8 mm (also predicting the effect of MLI placed on top of the CFRP), impacted by Al-projectiles with diameters in the range of between 0.7 mm and 1.2 mm, at normal incidence in the range of between 5.8 km/s and 6.6 km/s. The “no spall” curve estimation is to be validated.

4.3 Ballistic limit equations for H/C SP with CFRP face-sheets

In the first part of this chapter, four different ballistic limit equations for H/C SP with CFRP face-sheets are described. The equations are listed and their application is described.

Approach 1: BLE based on Whipple Shield Ballistic Limit Equation [7]

A common approach for calculating the Ballistic Limit Curves of H/C SP with CFRP face-sheets is to apply the Cour-Palais/Christiansen BLE [7] for metallic Whipple shields by:

- Substituting the CFRP face sheets with Al-plates having the same surface density (using e. g. the properties of Al 6061 T6 as a reference); and by
- Omitting the honeycomb core (spacing of the plates is then equal to the honeycomb core thickness).

This approach is frequently used for debris impact risk analysis [10]. For completeness, the equations used for the three velocity regimes are listed hereafter (the same notation as in [7] was used):

Ballistic limit diameter in the ballistic region ($v_n \le 3$ km/s):

$$d_c = \left[\frac{t_w \cdot (\sigma/40)^{0.5} + t_b}{0.6 \cdot (\cos\theta)^{5/3} \cdot \rho_p^{0.5} \cdot v^{2/3}} \right]^{18/19} \qquad (2)$$

Ballistic limit diameter in the transition region (3 km/s $< v_n <$ 7 km/s):

$$d_c = \left\{ \left[\frac{t_w \cdot (\sigma/40)^{0.5} + t_b}{1.248 \cdot \rho_p^{0.5} \cdot \cos\theta} \right]^{18/19} \cdot \left(1.75 - \frac{(v \cdot \cos\theta)}{4} \right) \right\} + \left\{ \left[1.071 \cdot t_w^{2/3} \cdot \rho_p^{-1/3} \cdot \rho_b^{-1/9} \cdot S^{1/3} \cdot (\sigma/70)^{1/3} \right] \cdot \left(\frac{(v \cdot \cos\theta)}{4} - 0.75 \right) \right\} \qquad (3)$$

Ballistic limit diameter in the hypervelocity region ($v_n \ge 7$ km/s):

$$d_c = \left\{ 3.918 \cdot t_w^{2/3} \cdot \rho_p^{-1/3} \cdot \rho_b^{-1/9} \cdot (v \cdot \cos\theta)^{-2/3} \cdot S^{1/3} \cdot (\sigma/70)^{1/3} \right\} \qquad (4)$$

For application of this equation to the case of CFRP H/C SP, the following values have to be assigned to the variables in Eq. (2)- (4):

- $t_w = t_b = t_{F/S,CFRP} * \rho_{CFRP}/\rho_{Al}$
- $S = t_{H/C}$
- $\sigma = \sigma_{y,Al}$
- $\rho_b = \rho_{Al}$

For the properties of Al the properties of e. g. Al 6061 T6 as listed in [11] can be used.

Approach 2: BLE based on Frost [6]

Frost et al. [6] report on impact tests on sandwich panels from AXAF, having face-sheets from graphite fiber reinforced polyimides ("GFRP") and aluminium honeycomb. The samples were covered with MLI. For the face-sheet materials carbon fibers M60J with 954 epoxy and P100 carbon fibers were used. A total of 18 test results are reported. Face-sheet thicknesses were varied between 0.254 mm and 1.524 mm. The

honeycomb thicknesses ranged between 6.35 mm and 15.875 mm having cell diameters of 3.175 mm and 0.254 mm. Projectile diameters ranged between 0.7938 mm and 3.175 mm. Impact occurred normal to the target surface, with impact velocities between 6.38 km/s to 7.26 km/s.

The ballistic limit equation for Whipple shields valid in the hypervelocity regime ($v_n \geq 7$ km/s, see Eq. (4)) was used to compare the test data. In this approach, the honeycomb core was omitted while the H/C core thickness was set as the spacing S in Eq. (4). Front and rear face-sheets of the CFRP H/C SP correspond to the bumper and the rear wall of the Whipple shield. Frost et al. [6] suggest two different approaches for the application of Eq. (4) to a CFRP H/C SP, for which they received approximately the same quantitative results. Only approach number 1 will be further analyzed here.

In Frost's approach no. 1, Eq. (4) is used with the composite material properties and the face-sheet thickness as if they were aluminium. The approach requires the yield strength and the density of the CFRP face-sheet. These data were not provided in [6] and are not readily available for specific CFRP designs. However the Frost approach is the only one of the four approaches discussed in this paper that considers actual basic material properties of CFRP.

In this paper, Frost's approach is extended to the transition region and the low-velocity region as well. Thus, for application of the Frost approach to the case of CFRP H/C SP, the following values have to be assigned to the variables in Eq. (2)- (4):

- $t_w = t_b = t_{F/S,CFRP}$
- $S = t_{H/C}$
- $\sigma = \sigma_{y,\,CFRP}$
- $\rho_b = \rho_{CFRP}$

For the CFRP face-sheets that were used in [6] no material data were supplied. Thus, to allow for approximation of the yield strength of the CFRP, a few assumptions had to be made:

1. tensile strength and yield strength of the laminate have the same value
2. the fibers are oriented unidirectional in each ply
3. the ratio of fiber volume to matrix volume amounts to 0.65 : 0.35. It is assumed that the matrix does not contribute tensile strength to the laminate.
4. the lay-up of the laminate is quasi-isotropic, having a stacking sequence of (0°/+45°/90°/-45°). Furthermore it is assumed that the layers in ±45° orientation contribute only 10% of their strength to the strength in either 0° or 90° direction. Layers orthogonal to the tensile direction do not contribute strength to the laminate.

Using these assumptions, the laminate strength can be calculated by multiplying the fiber strength with a factor of 0.195.

Thus, for the P100 graphite epoxy fiber laminates, which were used in [6] (see also Table 5), a laminate strength of 429 MPa would be expected assuming a fiber strength of 2.2 GPa.

Approach 3: BLE based on Taylor [5]

Taylor et al. [5] report on impact tests on sandwich panels with 1.62 mm thick CFRP face-sheets and 45 mm thick Al honeycomb core. Projectiles were aluminium, steel, nylon and titanium spheres (0.8 mm – 2 mm) tested over a velocity range of 4 - 6 km/s.

Based on the analysis of the impact test results, a ballistic limit equation based on the Christiansen/ Cour-Palais equation (Eq. (2), (3), and (4)) was developed by introducing a scaling factor for the thickness of the CFRP face-sheet. According to this approach, first the equivalent thickness of aluminium for the CFRP face-sheets has to be calculated based on the surface densities of CFRP and aluminium. Then the calculated aluminium rear wall thickness is to be multiplied with a scaling factor. The scaling factor suggested was 0.5 based on the analysis of the test data. The honeycomb core depth was set equal to the Whipple shield spacing S. The effects of the honeycomb were omitted.

For application of this approach to CFRP H/C SP, the following values have to be assigned to the variables in Eq. (2)- (4):

- $t_b = t_{CFRP} * \rho_{CFRP}/\rho_{Al}$
- $t_w = 0.5 * t_b$
- $S = t_{H/C}$
- $\sigma = \sigma_{y,Al}$
- $\rho_b = \rho_{Al}$

In [5], the yield strength values to be used in Eq. (2) and Eq. (4) were proposed to be set to 40 ksi and 70 ksi, respectively. However, Eq. (2) - Eq. (4) use only a single yield strength parameter (rear wall yield strength). Also, in this reference, no indication is made concerning the density of the reference Al-alloy to be used. In order to be consistent with Approach 1 described above, a different procedure is proposed to be used here: Thus, it is suggested to use the design properties of Al 6061 T6 for of ρ_{Al} and $\sigma_{y,Al}$ from [11] as a reference.

Approach 4: BLE based on EMI's Modified ESA Triple Wall (MET) equation

In [9], a ballistic limit equation for honeycomb sandwich panels from aluminium was derived and validated. The approach was to modify slightly the ESA Triple Wall BLE [10], which is frequently used in space debris risk analysis.

The ESA triple wall equation is a ballistic limit equation originally designed for application with metallic Whipple Shields. However, it has two coefficients (K3S and K3D) that can be adjusted to allow its application to ballistic limit curve calculations for other structures. It should be mentioned that the ESA Triple Wall equation is exactly the same as the Christiansen Whipple shield equation [7] for K3S = 1 and K3D = 0.16. However, in contrast to the Christiansen equation, no limit angle (angle where the ballistic limit projectile diameter does not increase any further for increasing impact angle) was defined in [10] for the ESA Triple Wall Equation.

The ESA Triple Wall Equation (ETW) was modified in [9] for application to *Aluminium* H/C SP. The modified ETW was denoted by "Modified ESA Triple Wall Equation" (MET). The modifications of the ESA Triple Wall Equation (ETW) suggested in [9] for application of this equation to *Aluminium* H/C SP structures consisted of:

- Modification of the angle dependence of the ESA Triple Wall Equation in the range $v_n<v_1$ (low velocity regime): instead of using $d_c \propto (\cos\theta)^{-5/3}$ in the ESA Triple Wall Equation the angle dependence is described in the Modified ESA Triple Wall equation by $d_c \propto (\cos\theta)^{-2/3}$. This describes the effect of the honeycomb core.
- Fitting of the coefficients K3S and K3D to experimental results obtained from impact tests on ROSETTA, METOP and ATV H/C SP from Aluminium. It was found that the data could be fit conservatively to coefficients K3S = 0.7 and $K3D = 0.0767 + 0.1833 \cdot t_{fs}$, where t_{fs} is the thickness of the front face-sheet of the Al-honeycomb sandwich panel (in units of [mm]).
- Setting equal the honeycomb core thickness with the standoff distance used in the ETW equation
- Consideration of MLI on top of the sandwich panel in the equations by effectively increasing the front face-sheet thickness with an amount of aluminium equal to the surface weight of the MLI.

This approach is used in this paper as a baseline for the ballistic limit equation for *CFRP* H/C SP. The following steps are to be followed to apply this equation to the case of CFRP H/C SP:

- Calculate the thickness of Al-face-sheets having the same surface density as the CFRP face-sheets using the appropriate volumetric density for CFRP (e. g. 1.77 g/cm^3 for ENVISAT CFRP). For the material properties of the reference aluminium alloy use the values for Al 2024 T81 alloy sheet material (0.010 - 0.249 inch thick) from MIL HDBK 5 [11]: Yield strength σ_y (Al 2024 T81) = 410.3 MPa, ρ(Al 2024) = 2.78 g/cm^3.
- In case MLI is used on top of the SP, calculate the thickness of an Al-plate having the same surface density as the MLI assuming ρ_{Al}=2.78 g/cm^3. Add the thickness to the front face-sheet thickness.
- Set equal the honeycomb core thickness to the standoff distance used in the ETW equation
- Use K3S = 0.70 and $K3D = 0.0767 + 0.1833 \cdot t_{F/S}$. $t_{F/S}$ (in units of [mm]) is the front face-sheet thickness of the equal surface density Al-plate (without MLI).

In order to apply this equation to CFRP H/C SP, it is obvious that some initial fitting will be needed to adjust the data to existing impact tests. This is because:

- The ESA Triple Wall equation was not designed to directly be applied to H/C SP
- The equation was not designed to be used for CFRP materials

To this purpose the entire equation was multiplied with a factor g_i, describing the type of failure:

- g_1 is the factor for describing the failure limit "no detached spallation" from the rear face-sheet of the CFRP sandwich panel
- g_2 is the factor for describing the failure limit "no hole" in the rear face-sheet of the CFRP sandwich panel

The g_i factors have been fitted against the impact test data from the ENVISAT structure wall listed in Table 3.

The complete set of equation is shown below (Eq. (5)-(7)).

Ballistic limit diameter in the ballistic region ($v_n \le 3$ km/s):

$$d_c(v) = g_i \cdot \left[\frac{\frac{t_w}{K_{3S}} \cdot \left(\frac{\sigma}{40}\right)^{1/2} + t_b}{0.6 \cdot (\cos\theta)^{5/3} \cdot \rho_p^{1/2} \cdot v^{2/3}} \right]^{18/19} \qquad (5)$$

Ballistic limit diameter in the transition region ($3\ km/s < v_n < 7\ km/s$):

$$d_c(v) = g_i \cdot \left\{ \begin{array}{l} d_c(v_1) \cdot \left(1.75 - \frac{v \cdot \cos\theta}{4}\right) + \\ + d_c(v_2) \cdot \left(\frac{v \cdot \cos\theta}{4} - 0.75\right) \end{array} \right\} \qquad (6)$$

$$v_1 = \frac{3\,km/s}{\cos\theta}$$

$$v_2 = \frac{7\,km/s}{\cos\theta}$$

Ballistic limit diameter in the hypervelocity region ($v_n \geq 7\ km/s$):

$$d_c(v) = g_i \cdot \left\{ \frac{1.155 \cdot t_w^{2/3} \cdot S^{1/3} \cdot \left(\frac{\sigma}{70}\right)^{1/3}}{K_{3D}^{2/3} \cdot \rho_p^{1/3} \cdot \rho_b^{1/9} \cdot (v \cdot \cos\theta)^{2/3}} \right\} \qquad (7)$$

The parameter list to be used with Eq. (5)-(7) is summarized in Table 8.

Table 8. Parameter list for EMI's MET (Eq. (5)-(7)) when applied to H/C SP with CFRP face-sheets (with and w/o MLI)

para-meter	description	Value to be used in Eq. (5)-(7)
ρ_b	density of reference Al-alloy (Al 2024)	2.78 g/cm^3
σ_y	yield strength of ref. Al-alloy (Al 2024 T81)	410.3 MPa (59.5 ksi)
t_b	front face-sheet thickness	$t_{F/S,CFRP} \cdot \frac{\rho_{CFRP}}{2.78} + \frac{\rho_{AD,MLI}}{2.78}$
t_w	rear face-sheet thickness	$t_{F/S,CFRP} \cdot \frac{\rho_{CFRP}}{2.78}$
S	spacing between front and rear face-sheet	$t_{H/C}$
K3S	fit factor for MET Equation [no units]	0.70 (for CFRP H/C SP)
K3D	fit factor for MET Equation [no units]	$0.0767 + 0.1833 \cdot t_{F/S}$, $t_{F/S}$ in [mm], where $t_{F/S} = t_{F/S,CFRP} \cdot \frac{\rho_{CFRP}}{2.78}$
g_1	factor describing failure mode "no detached spall" in rear face-sheet of H/C SP	$g_1 = 0.65$ (fitted to ENVISAT impact test results)
g_2	factor describing type of failure "no hole"	$g_2 = 0.83$ (fitted to ENVISAT impact test results)

4.4 Comparison of the predictions from ballistic limit equations for CFRP H/C SP with experimental data

In this chapter, the ballistic limit predictions are for CFRP H/C SP are compared with results from impact test data. The first subchapter contains the material parameters used in the calculations. These parameters are to be used together with the equations listed in Chapter 4.3. The other paragraphs contain the comparison between the predictions from the four ballistic limit equations derived in Chapter 4.3 compared with the test data listed in Chapter 3. Also, refer to Chapter 3 for the descriptions of the samples.

Material data used in the equations

Approach 1 and Approach 4 require the yield strength and density of Al 6061 T6 and Al 2024 T81, respectively, as a reference. This data, taken from [11], are listed in Table 9.

Table 9. Material parameters of Al-alloys used as reference (from [11])

parameter	Al 6061 T6*	Al 2024 T81*
ρ	2.71 g/cm^3	2.78 g/cm^3
σ_y	(36.5 ksi) 251.7 MPa	(59.5 ksi) 410.3 MPa

* for sheets having thickness of 0.010-0.249 inch, average from L and LT directions

Approach 2 requires the density and strength of CFRP. The values used for the calculations are listed in Table 10.

Table 10. Material parameters of CFRP

parameter	AXAF satellite CFRP - P100 fiber laminate	Taylor CFRP CFRP HMF371	ENVISAT CFRP M40
ρ	1.77 g/cm^3 (3)	1.825 g/cm^3 (5)	1.77 g/cm^3 (3)
σ_U/fiber (1)	2.2 GPa (4)	2.758 GPa (6)	2.740 GPa (7)
σ_U/laminate (2)	459 MPa	538 MPa	534 MPa

(1) it is assumed that the yield strength required by the BLE can be substituted with the value for the upper tensile strength of the laminate

(2) the laminate tensile stress has been calculated using the assumptions listed in Chapter 4.3 (see Approach 2)

(3) assumed value

(4) from www.goodfellow.com

(5) average value from [5]

(6) In [5], no data was provided concerning the tensile strength of the fibers used. In the following it is assumed that the fiber HMF371-7714B is a high modulus fiber having a tensile strength of 400 ksi (= 2758 MPa), which is a typical value for HM fibers

(7) from www.torayusa.com

An areal density of 0.056 g/cm^2 was used for the ENVISAT MLI (taken from [4]). The areal density

value of the MLI used on the AXAF samples was not published in [6]; it is assumed that the areal density amounts to 0.05 g/cm^2.

For the projectile density a value of 2.80 g/cm^3 was assumed (density of Al 7075).

In the following, the predicted ballistic limit curves from the four different approaches are plotted against the available impact test results. For ease of notation, Approach 1 from Chapter 4.3 (BLE based on Whipple Shield BLE") is denoted by "Christiansen".

ENVISAT impact test data and predictions

The data from HVI tests on ENVISAT CFRP H/C SP are summarized in Table 3. The ballistic limit curves are plotted versus the experimental data in Fig. 9 - Fig. 11.

In Fig. 9 Frost's, Christiansen's, and Taylor's approach have been plotted against the test results of ENVISAT samples without MLI. Frost's approach and application of Christiansen's equation overpredict the ballistic limit projectile diameter. Frost's approach yields unrealistically high critical projectile diameter throughout the velocity range from 0 to 15 km/s. Thus, neither of these approaches is suitable for assessing the ballistic limit diameter of the ENVISAT CFRP H/C SP.

The ballistic limit curve for Taylor's approach shows a good agreement with the experimental data.

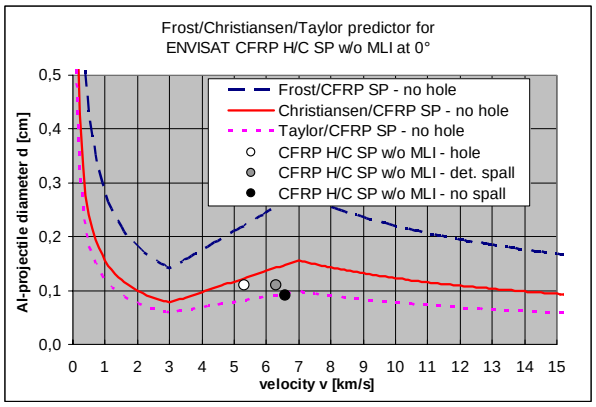

Fig. 9. ENVISAT CFRP-H/C SP w/o MLI; experimental data and calculated BLC for 0° impact using predictions from Frost, Christiansen, and Taylor approach

In Fig. 10, the MET curve is plotted against the test data. Note that this set of test data was used for fitting the curve parameters. The obtained parameters (g_1 and g_2, see Table 8) will be used as a baseline for all other CFRP H/C SP. The advantage of having the new ballistic limit equation is its capability to distinguish between two different failure modes: in some applications it is enough to apply the "no hole" failure threshold, in other applications a more sensitive failure threshold condition may be useful. This failure threshold (i. e. spall detachment from the rear face-sheet) marks the onset of ejection of finely fragmented carbon fibres and matrix material into the interior of the spacecraft, resulting in contamination of the interior spacecraft volume. This contamination could trigger electrical perturbations or other types of spacecraft anomalies as a result of the conductivity of the carbon fibres.

In Fig. 11, results of impact tests on ENVISAT CFRP H/C SP with MLI are plotted against the predictions from the MET equation. The predictions are slightly conservative.

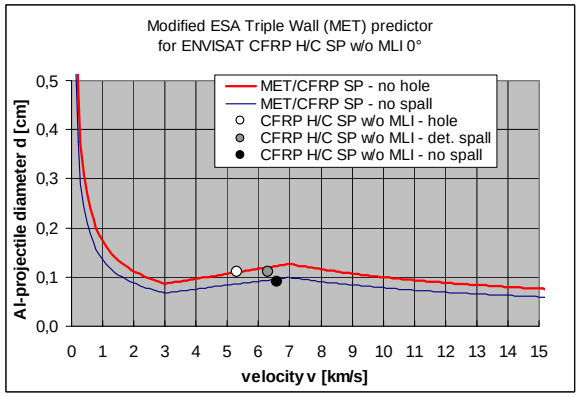

Fig. 10. ENVISAT CFRP-H/C SP w/o MLI; experimental data and calculated BLC for 0° impact using MET predictor

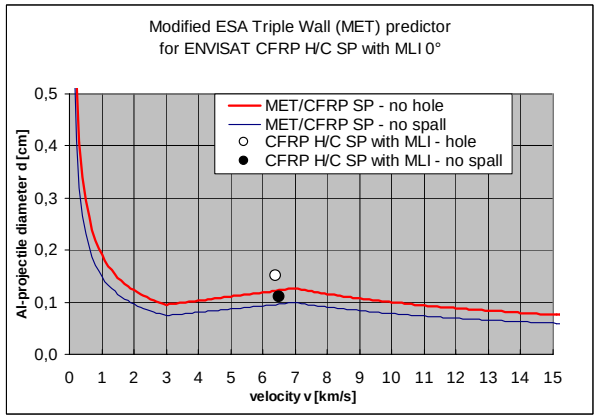

Fig. 11. ENVISAT CFRP-H/C SP with MLI; experimental data and calculated BLC for 0° impact using MET predictor

Taylor impact test data and predictions

The impact test data used in the following figures (Fig. 12 - Fig. 13) stem from Taylor et al. [5], see Table 4.

Fig. 12 shows the predicted ballistic limit curves of Frost, Christiansen, and Taylor. Again, the Christiansen

approach slightly overpredicts, and Frost's approach drastically overpredicts, the ballistic limit diameters. The Taylor equation makes the correct predictions, as this equation (Approach 3) was fitted to this set of data (in [5]).

The Modified ESA Triple Wall approach (approach 4 in Chapter 4.3) yields the ballistic limit curves shown in Fig. 13. For failure scenario "no hole", the curve makes the correct predictions of the test results. The investigators in [5] did not report any case of detached spall. Thus it cannot be checked whether the predictions from the "no spall" ballistic limit curve (Fig. 13) are correct.

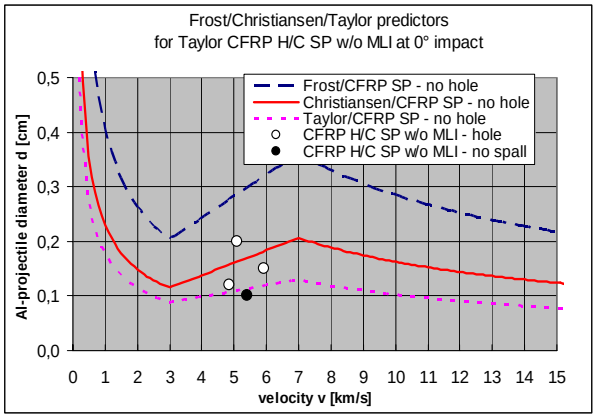

Fig. 12. Taylor HVI data on CFRP-H/C SP w/o MLI; experimental data and calculated BLC for 0° impact using predictions from Frost, Christiansen, and Taylor approach

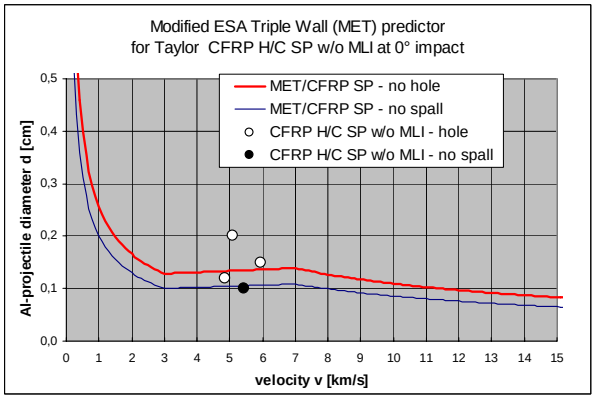

Fig. 13. Taylor HVI data on CFRP-H/C SP w/o MLI; experimental data and calculated BLC for 0° impact using MET predictor

AXAF impact test data and predictions

The AXAF impact test data is presented in Table 5.

The test data and the predictions from Frost's, Christiansen's and Taylor's approach are shown in Fig. 14. For the two tests at approximately 7 km/s, the Christiansen and Taylor methods make conservative predictions. Note that Frost's equation has originally been fit to this specific data set.

In Fig. 15, the MET equation is plotted against the AXAF impact test data. It is obvious that this equation underpredicts the actual ballistic limit diameter at 7 km/s. However, this is more favourable than overpredicting.

Thus, for the AXAF samples, all equations make useful (to a varying degree) predictions when comparing to the two test data.

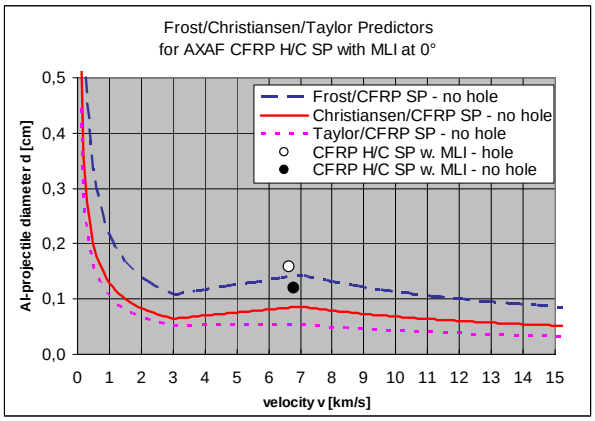

Fig. 14. AXAF HVI data on CFRP-H/C SP w/o MLI; experimental data and calculated BLC for 0° impact using predictions from Frost, Christiansen, and Taylor approach

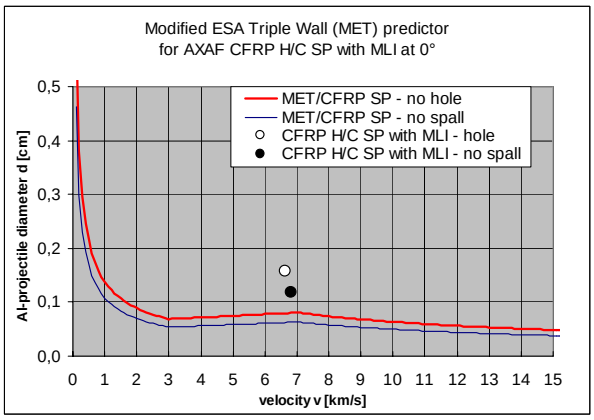

Fig. 15. AXAF HVI data on CFRP-H/C SP w/o MLI; experimental data and calculated BLC for 0° impact using MET predictor

It is obvious that MET and Taylor's approach make good predictions for CFRP H/C SP with large H/C core thickness and fairly thick face-sheets. Frost's approach is well suited to thin CFRP H/C SP with thin face-sheet.

5. SUMMARY AND CONCLUSIONS

In this paper ballistic limit equations for CFRP structure wall of satellites have been presented. All ballistic limit equations for CFRP plates and CFRP H/C SP have been based on limit equations originally developed for standalone metallic plates and spaced metallic plates. Thus neither special failure modes of CFRP (detatched spallation, clear perforation), nor the influence of the honeycomb core on the protection performance are considered. In order to properly describe the influence of fiber type, matrix, fiber-volume-content, lay-up, H/C core material/geometry, etc., systematic test campaigns on samples with well defined varitions in geometrical design and materials would be necessary.

For CFRP plates, a new ballistic limit equation was presented. This equation is based on the Cour-Palais Thin Plate equation for metallic plates. It considers two different types of failure modes - "no detached spall" from the rear side of the CFRP plate and "no hole" in the CFRP plate. It also considers the effect of MLI, placed on top of the plate, on the ballistic limit diameter.

Four different approaches for ballistic limit equations of honeycomb sandwich panels with CFRP face-sheets and Al-honeycomb core were investigated. Three of the equations consider only one failure scenario ("no hole"). The fourth BLE (MET - "Modified ESA Triple Wall Equation") allows a distinction between 2 different types of failure scenario: "no hole" and "no detached spall" in the rear CFRP face-sheet of the panel to be made.

Three sets of impact test data were used in this paper for comparison with the predictions from four different approaches for ballistic limit equations for CFRP H/C SP. It was found that Frost's approach and the Christiansen approach overpredict the ballistic limit diameters when applied to the ENVISAT and Taylor samples. This rules out their use in space debris risk analysis. Taylor's approach and the MET make good predictions to Taylor's data and ENVISAT data. For AXAF both approaches provide fairly conservative predictions. If distinction of "no spall" and "no hole" failure modes are required, the MET equation can be used.

On the whole there were very little suitable impact test data published that could be exploited for the paper. The same accounted for the limit equations. Clearly, this indicates that there have been an insufficient number of investigations on the hypervelocity impact behaviour of CFRP structures and related investigations.

7. ACKNOWLEDGEMENT

This study was performed in the frame of WP 2000 of ESA Contract 16721/02/NL/CK "Composite Materials Impact Damage Analysis"

8. REFERENCES

1. Lambert M., "Hypervelocity impacts and damage laws", Adv. Space Res., 1997, 19(2), 369-378

2. F. Schäfer, E. Schneider, "Hypervelocity Impacts on CFRP - Summary of Results", EMI Report CFRP 0001 for ESA/ESTEC, Ernst-Mach-Institute, Freiburg, Germany, 16. April 1996

3. J. Unda, J. Weisz, A. Uriarte , R. S. Capitanio, "Residual Strength of CFRP Tubes Subjected to Hypervelocity Debris Impact", 45th Congress of the International Astronautical Federation, October 9-14, 1994, Israel

4. M. Lambert, F. K. Schäfer, T. Geyer, “Impact Damage on Sandwich Panels and Multi-Layer Insulation“, Int. J. Impact Engng. 26 (2001) 369-380

5. E.A. Taylor, M.K. Herbert, B.A.M. Vaughan, J.A.M. McDonnell, “Hypervelocity impact on carbon fibre reinforced plastic/aluminium honeycomb: comparison with Whipple bumper shields”, Int. J. Impact Engng. 23 (1999)

6. C. L. Frost, P. I. Rodriguez, “AXAF Hypervelocity Impact Test Results”, Proc. Second European Conference on Space Debris, ESA SP-393, 1997

7. E. L. Christiansen, Design and Performance Equations for Advanced Meteoroid and Debris Shields, Int. J. Impact Engng., Vol. 14, pp. 145-156 (1993)

8. Hayashida, K. B. and Robinson, J. H., "Single Wall Penetration Equations", NASA TM-103565, 1991

9. F. Schäfer, S. Haas, "Preliminary evaluation of critical impact conditions leading to failure", WP 2420 of ESA Contract 16721/02/NL/CK Composite Materials Impact Damage Analysis, EMI report, June 2004, Fraunhofer EMI Freiburg, Germany

10. ESABASE/DEBRIS, Meteoroid/Debris Impact Analysis Technical Description, Issue 1 for ESABASE version 90.1, G. Drolshagen, WMA, J. Borge, Matra, January 1992

11. "Military Handbook, Metallic Materials And Elements For Aerospace Vehicle Structures", MIL-HDBK-5, January 1998, US Department of Defence